

The Development of a Hand-Launched Small UAV for Ground Reconnaissance

Paulo Iscold, Guilherme A. S. Pereira and Leonardo A. B. Torres

Abstract

The engineering design of a hand-launched small unmanned aerial vehicle – SUAV, together with real data from practical flight tests, is presented in this paper. The main goal achieved in this work was the implementation of a low cost, portable, and reliable aerial platform for ground reconnaissance. The vehicle was specially designed such that the number of necessary sensors and actuators was purposely reduced, nonetheless without precluding the feasibility of the assigned mission.

Index Terms

Unmanned Aerial Vehicles, guidance strategy, control design.

I. INTRODUCTION

The development of Unmanned Aerial Vehicle (UAV) systems has been recently the focus of many researches throughout the world. The importance of this kind of vehicle in aerial activities has grown continuously in the last years, especially for military and reconnaissance purposes, particularly in operations where the tasks are dangerous or tedious for human pilots.

In Brazil, many research centers have strived to develop UAV projects, including control and navigation systems, aerial platforms and specialized payloads. One of these research centers is Federal University of Minas Gerais – UFMG, where the Research and Development of Autonomous Vehicles – PDVA group has been dedicated to the development of UAVs. As part of the PDVA research effort, an aerial platform called AqVS was developed. This project

Corresponding author: torres@cpdee.ufmg.br

The authors are members of the PDVA research group at the Universidade Federal de Minas Gerais – UFMG.

has, as its main objective, the development of a small UAV (SUAV) for autonomous ground reconnaissance.

Autonomous ground reconnaissance is considered in the present paper to be a problem of flying the SUAV over a given sequence of waypoints. In this case, the vehicle is expected to approach each waypoint in an appropriate way such that the targets remain visible by an onboard video camera. In addition, it is very important that the system be portable, hand launchable, and able to fly in diverse weather conditions. Moreover, it is desirable to have an inexpensive aerial platform that, in the future, will be able to integrate a team of dozens of similar aerial vehicles.

From the above requirements, one can conclude that the main payload is a wireless camera used to transmit images to a fixed or moveable ground base, in which the images are processed. Although the transmitted images are not directly used in the control of the aerial robot, they are considered to be the main result achieved by the hand-launched SUAV.

Another consequence of the stated requirements is that limitations on size, energy consumption and payload weight certainly impose important constraints in the SUAV design. This is particularly true regarding the design of the control system structure, where processing capability has also to be considered carefully.

Commercially, there are important players in the development of off-the-shelf control systems for SUAVs, such as MicroPilot (1), CloudCap (2), and CrossBow (3). All of these systems have very small sizes, low weight, low energy consumption and adequate processing capabilities to be used in SUAV development. Regarding sensors, all of them have, basically, static and dynamic pressure for barometric altitude and airspeed measurements, GPS for localization, and micro-electromechanical (MEMS) accelerometers, gyroscopes and magnetometers to be used in attitude determination. Although this seems to be the minimum sensor solution for a SUAV, it is possible to propose alternatives that can reduce even more the number of sensors.

For example, although the use of MEMS based inertial measurements in conjunction with Kalman filters has been an alternative used in many works in the recent literature (4; 5; 6), there are other less computationally intensive options that can be explored, such as the use of GPS information (7), or attitude estimation based on infrared inclinometers (8; 9). Yet, another approach is to use computer vision for attitude estimation (10), which can become attractive if there is digital video stream available due to the very nature of the proposed SUAV mission. On the other hand, regarding altitude and airspeed measurements, although the use of pressure

sensors is the usual alternative, the fusion of inertial and GPS measurements can sometimes be used to increase the accuracy of altitude and airspeed estimates, or even to eliminate the need for dedicated pressure sensors.

In this context, despite the fact that the development of a formal procedure to design a guidance, navigation, and control structure able to comply with the above constraints may be considered as a major theoretical endeavor, the main contribution of this paper is to present a possible practical solution that relies on simple and effective strategies. Indeed, the SUAV, described in the next sections, has been considered to be a reliable system, developed with a good tradeoff among payload, complexity and cost.

The paper is organized as follows: in Section II an overview of the SUAV system is presented. The strategies used to guide the vehicle through pre-assigned waypoints are discussed in Section III. In Section IV, the design of an autopilot control structure is presented, which relies on a limited set of measurements, but it is capable of driving the vehicle to follow the velocity vectors generated by the proposed guidance strategies. The SUAV simulation environment and accompanying simulation results are presented in Section V. Real data from flight tests are presented and discussed in Section VI. In Section VII final remarks and conclusions related to the SUAV development are registered.

II. AERIAL PLATFORM DESCRIPTION

The development of the SUAV for ground reconnaissance was oriented toward an aerial platform with simple and reliable operational procedures. This can be translated to a small size, easy field assembling, low-noise, and clean engine aircraft system, which does not demand high level pilot skills. These features are found in the electrical motor glider aircraft model used in this work as the primary airframe, whose characteristics are listed in Table I.

The aircraft model was modified from an original Spirit 100 ARF¹ kit produced by Great Planes Model Inc. by adapting an electrical engine and through the construction of a cargo bay on the wing root (11), as shown in Fig. 1.

The aerial platform was also equipped with specific guidance, navigation and control (GN&C) hardware in order to fulfill its mission. This additional hardware, to be detailed in Section IV-C,

¹Almost Ready to Fly.

Table I
MODIFIED ELECTRICAL MOTOR GLIDER AIR MODEL CHARACTERISTICS.

Variable	Value
Total Weight	25 N
Wingspan	2 m
Length	1.6 m
Wing loading	27–29 N/m ²
Wing area	0.42 m ²
Operational ceiling	150 m (above ground level)
Cruise speed	13.9 m/s (50 km/h)

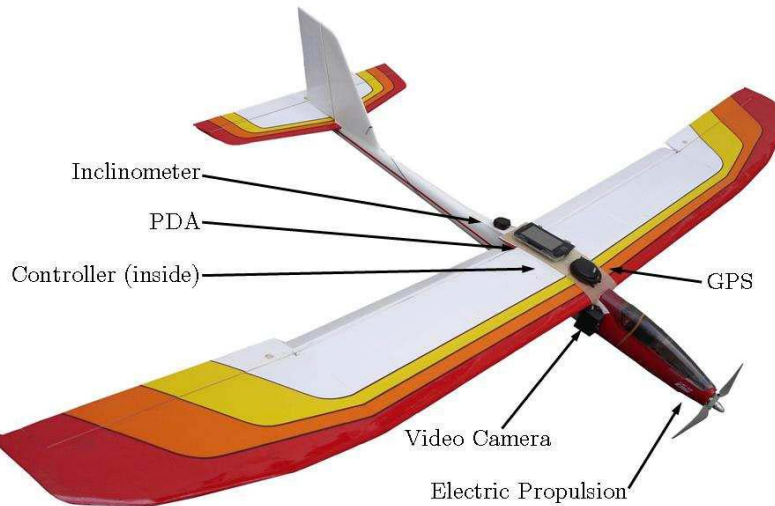


Figure 1. The aerial platform modified by the addition of an electrical engine system, a cargo bay to hold the mission oriented guidance, navigation and control hardware, and a video camera.

provides the elements depicted in Fig.2, comprising the set of sensors, actuators, and digital processing devices considered to be essential to reliably perform the ground reconnaissance task.

An interesting characteristic of the implemented aerial platform is the use of a Personal Digital Assistant (PDA) as the main digital processing device used to compute both reference trajectory

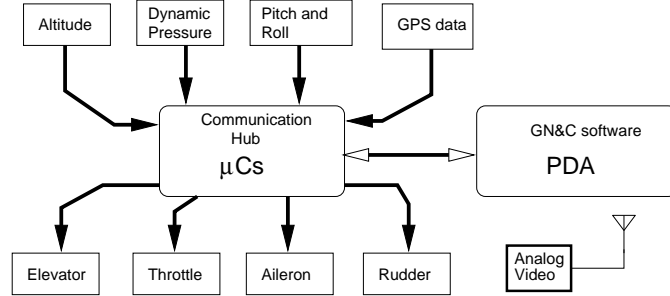


Figure 2. SUAV hardware overview. The main component is a PDA in which the guidance, navigation and control (GN&C) algorithms are executed. All the signals in the system go through a communication hub implemented using microcontrollers (μ Cs).

and corrective control action (Fig.2). This PDA is attached to the cargo bay before each flight. The experimental data is then downloaded from it after the landing of the aircraft for posterior analysis.

III. GUIDANCE STRATEGY

As mentioned before, in the present work ground reconnaissance is modeled as problem of flying the small UAV to approach, within a given radius r imposed by the camera field of view, waypoints specified from a sequence of targets to be filmed or photographed. At first, no constraints are imposed on the distribution of waypoints over a given region. However, it is assumed that a higher level planning have taken into account the kinematics constraints of the vehicle, such as the minimum UAV turning radius, when choosing the sequence of waypoints. This higher level planning is not discussed in this paper.

Although several methodologies based on trajectory following have been proposed for UAV guidance (12; 13), vector field based methodologies were applied to guide the UAV in this work. These methodologies are based on the determination of a vector field over the airplane workspace such that the integral curves of the vector field define implicit paths from every initial UAV position to the target. The robotics literature have been shown that this fact leads to methodologies that are very efficient to be computed on the fly, robust to small pose estimation errors, and that present good final paths. Besides these advantages, vector fields based methodologies, such the ones based on the gradient of an artificial potential functions (14), have been extensively used to control ground mobile robots, mainly because they allow the combination of

planning and control in the same solution. This fact yields in provable correct solutions for the motion planning problem since, frequently, the potential functions may be considered as natural Lyapunov candidate functions for closed loop analysis (15; 16).

A clear drawback of such methodologies is that, in opposition to the traditional methods based on trajectory following, vector fields based approaches do not impose time constraints to the flight, but only orient the aircraft to the correct position. Also, as will be pointed in the next subsections, the specific approaches used in this work do not guarantee that the aircraft will follow a previously specified path but, instead, will constrain the flight to a region of the workspace. Although these facts may impose difficulties for some specific tasks, they are suitable for the current surveillance mission the AqVS UAV is performing, as will be shown in Section VI. The next two subsections present the two vector field methodologies evaluated in this paper.

A. Switched Vector Field

Consider that waypoints relative to the mission targets are given by a sequence of configurations $\mathbf{Q} = \{\mathbf{q}_1, \mathbf{q}_2, \dots, \mathbf{q}_n\}$, where $\mathbf{q}_i = [x_i, y_i] \in \mathbb{R}^2$. Each configuration is expressed in a fixed reference frame $\{W\}$, with origin at \mathbf{q}_1 , and the xy plane is assumed to be tangent to the earth, with y axis pointing north. Notice that only the planar positions of the waypoints are considered. Therefore, either the waypoints are constrained to a constant altitude or their altitudes are considered separately as inputs for the altitude controller presented in the next section.

A simple and very well known approach for waypoint navigation using vector fields is to compute an attractive vector field to the next waypoint to be reached. Mathematically, for each waypoint at configuration $\mathbf{q}_i = [x_i, y_i]$ it is defined an attractive potential function given by:

$$\Phi_i(\mathbf{q}) = \frac{1}{2}\alpha d^2(\mathbf{q}), \quad (1)$$

where $\mathbf{q} = [x, y]$ is the UAV current configuration, d is the Euclidean distance between \mathbf{q} and \mathbf{q}_i and α is a positive constant. The UAV will eventually reach \mathbf{q}_i if it follows the negated gradient of Φ_i given by:

$$\mathbf{u}_i(\mathbf{q}) = -\alpha[x - x_i, y - y_i]. \quad (2)$$

Notice that the quadratic function Φ_i do not need to be computed by the vehicle, that only need to compute $\mathbf{u}_i(\mathbf{q})$ on the fly. At first, the orientation of $\mathbf{u}_i(\mathbf{q})$ is considered to be the desirable UAV heading, and its magnitude the UAV speed setpoint. If it is desirable that the UAV presents

a constant linear velocity, one may use the normalized gradient with similar results. It is also important to say that Φ_i is a Lyapunov Function candidate for the stable point \mathbf{q}_i and can be used to prove the robot convergence to this waypoint. This is easily done, for instance, if it is considered a vehicle with simple integrator dynamics $\dot{\mathbf{q}} = \mathbf{u}_i(\mathbf{q})$.

Once \mathbf{q}_i is achieved, within a given proximity radius, a new vector field is computed for the next waypoint. This process continues until the whole set of waypoints is visited, when the process may start from the first waypoint again.

As pointed out in (17), the big issue with this methodology is the discontinuity that appears in the composite vector field when the waypoints are switched. Since the vector field is the input for a lower level controller, discontinuities are not desirable in the sense that they may cause significant overshoots in the robot path, what may not be acceptable when the distance between two waypoints is of the order of magnitude of the UAV turning radius. However, this simple methodology is very robust and efficient, what is very suitable for low processing capabilities systems. The next subsection presents another vector field approach that was proposed in order to avoid the discontinuity in the field.

B. Continuous Vector Field

A second and more elaborated proposal for vector field guidance is inspired by the field of hybrid (continuous + discrete) systems. Such systems have already been used to solve robot navigation problems (18; 19). However, to the best of the authors knowledge, this is the first time this methodology is applied to guide an aerial vehicle.

The basic idea of the method is to construct a polygonal corridor that contains the whole set of waypoints specified by the task and to compute a continuous vector field inside the corridor. Observe that this idea is also very interesting when the targets to be surveilled form natural corridors, such is the case of roads, pipes, transmission lines, etc. A clear advantage of this methodology over other vector fields methodologies already used to guide UAVs (15; 16) is the simplicity to generate non-convex paths with guaranteed continuity of the field inside the polygonal corridor.

The method begins with the computation of the polygonal corridor using a geometric method. The second step consists in the triangulation of the corridor, what yields in a discrete environment with a finite number of triangular cells. Notice that, both corridor computation and triangulation

are executed off-line and, therefore, are not subject to the system hardware limitations. Figure 3(b) shows an example of triangulated closed corridor around the set of four waypoints in Figure 3(a).

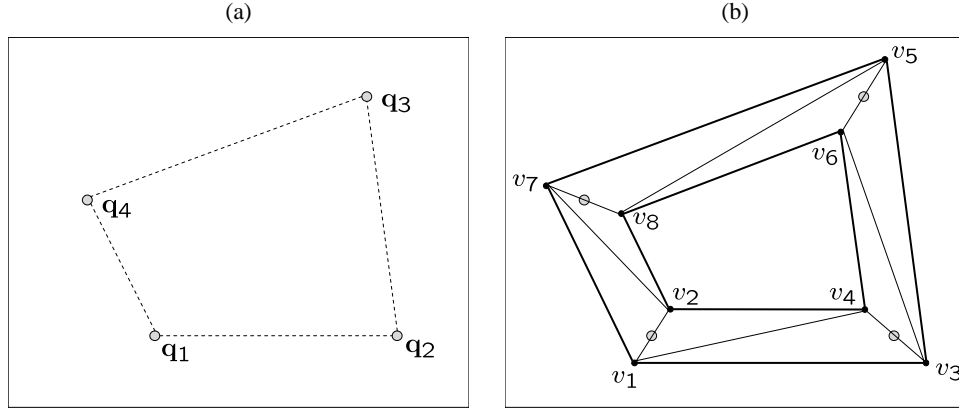


Figure 3. (a) – A set of waypoints forming a polygon. (b) – A triangulated corridor containing the waypoints.

Finally, in order to obtain the field inside the corridor, the methodology presented in (20) is used. In this method, the computation of the vector field depends on the choice of a set of base vectors, one for each vertex of the corridor. Once the base vectors are computed, the vector field in configuration \mathbf{q} inside each triangle is computed by the convex combination of the three vectors at the vertices of the triangle given by:

$$\mathbf{u}(\mathbf{q}) = \frac{A_i \mathbf{u}_i + A_j \mathbf{u}_j + A_k \mathbf{u}_k}{A_i + A_j + A_k}, \quad (3)$$

where A_i , A_j , and A_k are the areas of the sub-triangles formed between the original vertices of the triangles and point \mathbf{q} as shown in Figure 4, and \mathbf{u}_i , \mathbf{u}_j , and \mathbf{u}_k are the vertices' base vectors. Notice that, since two adjacent triangles share two base vectors (the ones at the common edge), the field is continuous between two triangles.

Although the computation of the field inside the corridor is simple, the choice of the base vector is critical and essential to guarantee that the resultant field will keep the aircraft inside the corridor and moving in the correct direction. As pointed in (20) any vector that has both negative projection on the outward normal vectors of the corridor boundaries and positive projections on the outward normal vectors of intersection edge between two consecutive triangles could be chosen. The only problem in this case is that, due to geometric characteristics, not always both

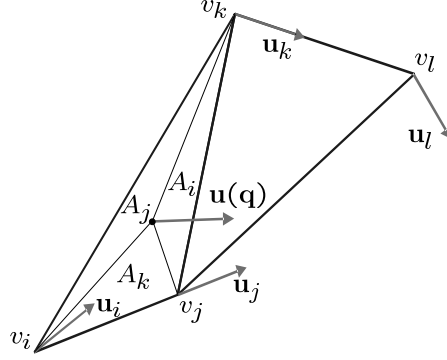


Figure 4. The convex combination of the base vectors of each triangle generate a vector field inside the triangle. Since two consecutive triangles share two vectors, the vector field is continuous inside a sequence of triangles.

constraints can be satisfied (18). In this cases, as proposed in (20), one or two triangles are to be created and a non-fixed vector must be used. Details of this methodology can be found in (20).

As proved in (20), if this algorithm is used, a vehicle with dynamics given by $\dot{\mathbf{q}} = \mathbf{u}(\mathbf{q})$ will be constrained to move inside the corridor. However, since the actual UAV is subjected to non-holonomic constraints and disturbances, such wind, it may scape the corridor. In this situation, a vector field must be created to force the vehicle to fly inside the corridor again. In this paper it is proposed to use a simple, radial vector field that points towards the borders of the corridor. Unfortunately, this external field introduces a discontinuity at the border of the corridor, which affects the UAV behavior when it flies outside the corridor.

It is important to say that in both vector fields methodologies presented in this section, the field itself is not computed *a priori* for the whole environment. Instead, each vector is computed online for a given robot configuration \mathbf{q} using Equations (2) or (3). Also, it is important to design a set of controllers to make the vehicle to track the vector field. The controllers used by the AqVS SUAV are presented in the next section. As presented next, these controllers use as reference signal the desired course given by the direction of vector $\mathbf{u}(\mathbf{q}) = [u_x, u_y]$ computed as $\psi_{\text{ref}} = \arctan(u_y/u_x)$, and the dynamic pressure, which may be derived from the vector magnitude.

IV. CONTROL STRUCTURE DESIGN

The choice of appropriate control laws is critical in the development of SUAVs because the number of sensors and the computational capacity is usually very limited. In this project, the

control actions are calculated as separate control laws, corresponding to longitudinal and latero-directional aircraft dynamic modes.

This separation of aircraft dynamics, usually considered to be a valid assumption in aircraft control systems, is acceptable as long as the sideslip angle (which represents the intensity of lateral velocity in relation to the atmosphere) and the bank angle are small (21). Although in the present case of a modified glider aircraft model driven by the guidance strategy discussed in Section III this is not at all true during all phases of flight, such hypothesis greatly simplifies the control laws tuning process. Deviations from this natural decoupling condition were considered to be unavoidable model disturbances that should be overcome by adequate feedback and/or feedforward of relevant state variables; i.e. by appropriate control structure design; as it will be presented below.

In order to further simplify the process of finding suitable control parameters, each control law was implemented following a multiloop approach; i.e. a decentralized structure; which has the advantage of being more amenable to inclusion of pilot knowledge (operator skills) to improve the vehicle overall performance.

The controllers parameters were determined by following two major steps: gross adjustment based on stability requirements; and fine tuning by means of a trial-and-error evaluation procedure from simulated results.

Very simple strategies were used in the tuning process to achieve SUAV closed loop stability. This task was carried out by analysing independently the longitudinal and latero-directional SUAV dynamical behaviors. This was done by means of: (i) linearization of the SUAV mathematical model around different equilibrium flight conditions; (ii) balanced model reduction for longitudinal and latero-directional open-loop state space models; and (iii) parameters tuning of PID and internal stability augmentation loops performed by closing one loop at a time, and relying on frequency domain and root locus based SISO control design techniques, such that each transfer function relating pairs of actuator signals to output variables was considered separately.

In the fine tuning procedure, the controllers parameters were adjusted in order to improve step responses related to abrupt variations in speed, altitude and yaw/course angle reference signals. In this case, simulation results obtained considering the complete nonlinear aircraft model (to be discussed in Section V) were used. Maximum overshoot and settling time were the primary measures used to evaluate the controllers performance. Also, during this procedure, static

feedforward gains used in the longitudinal and latero-directional control structures, described in the following sections, were also determined.

A. Longitudinal Control Law

For the longitudinal controller, as shown in Fig.5, two PID loops were implemented: altitude h control, and dynamic pressure P_{dyn} (speed) control.

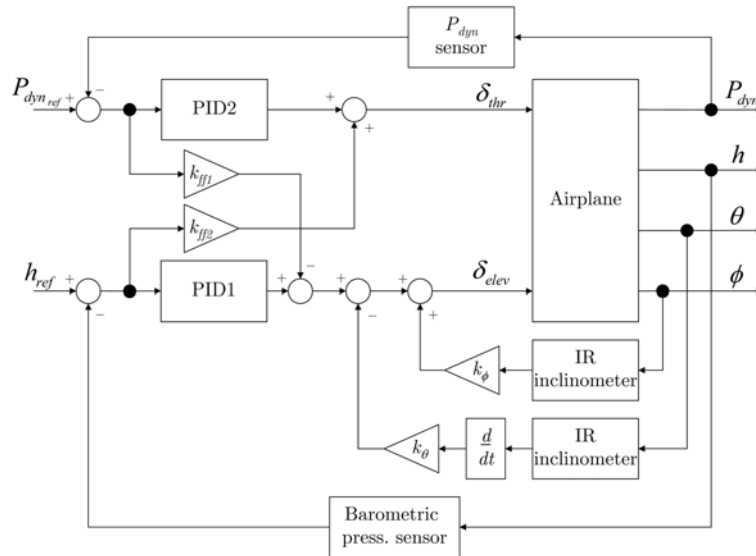


Figure 5. Decentralized longitudinal control approach. Two outer PID control loops are used to keep altitude h and dynamic pressure P_{dyn} (speed) at desired levels. Internal stability augmentation based on pitch rate $d\theta/dt$ feedback, and feedforward from bank angle ϕ to elevator deflection δ_{elev} , were also employed to improve the altitude control loop performance.

In the altitude control loop, the output is measured from a high resolution digital baro-altimeter, and elevator deflection δ_{elev} is issued as the corrective action. To improve the altitude dynamic response, while keeping the aircraft stable, a stability augmentation internal loop was added, based on pitch rate estimation, obtained from differentiating the filtered measurement of pitch angle θ from an infrared inclinometer. Additionally, a feedforward path from wing bank angle ϕ to elevator deflection δ_{elev} was added in order to minimize the altitude loss during curves, which partially circumvents the effect of incomplete longitudinal and latero-directional decoupling, for significant bank angles.

In the dynamic pressure control loop, the difference between the total pressure at the entrance of a small forwardly directed tube and the ambient (static) pressure is measured as an indication

of the square of the aircraft speed, which is related to the dynamic pressure P_{dyn} defined by

$$P_{\text{dyn}} = \frac{1}{2} \rho S_w V_T^2, \quad (4)$$

where ρ is the air density, S_w is the SUAV wing area, and V_T is the total speed of the vehicle with respect to the atmosphere. This measurement is then fed-back and used to vary throttle position δ_{thr} to compensate for aircraft speed variations, by varying the forward thrust force provided by the electrical engine system.

Once the speed and altitude state variables in an aircraft during flight are intrinsically related through the natural exchange of kinetic and potential energies, respectively, two feedforward control paths, implemented by using static gains $k_{\text{ff}_1} \neq 0$ and $k_{\text{ff}_2} \neq 0$, were added to partially decouple the individual altitude and dynamic pressure control loops. An example, in which case the use of such decoupling feedforward gains is important, is when the aircraft loses altitude due to two very different mechanisms: (i) by reaching the stall condition (low speed and high angle of attack, together with abrupt reduction in lift force); and (ii) by rapidly diving with increasing dynamic pressure (increasing speed and low angle of attack). In the first case the correct action is to increase the thrust force without augmenting the elevator deflection, which would be a potentially dangerous operation once the aircraft is near stall. In the second case, the preferred movement is to deflect the elevator without changing thrust power, which increases pitch angle and decreases dynamic pressure. These appropriate actions are effected by relying on the aforementioned feedforward static gains.

B. Latero-directional Control Law

The AqVS SUAV uses a bank-to-turn flight strategy, i.e. the inclination of the SUAV wings, effected by ailerons deflection δ_{ail} , allow the vehicle to perform curves such that the vector field provided by the guidance strategy can be followed (Section III).

As shown in Fig.6, the latero-directional controller is composed by a yaw/course angle ψ outer PI controller, together with an inner PID loop for bank angle ϕ regulation.

The outer loop is responsible to generate a reference roll angle ϕ_{ref} , from the difference between desired yaw/course angle ψ_{ref} and measured course angle ψ provided by an airborne GPS receiver.

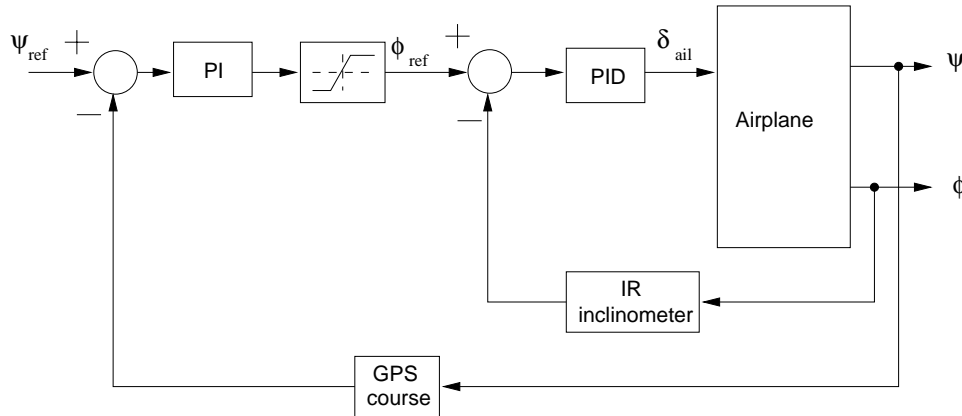


Figure 6. Latero Directional control diagram. An outer loop based on GPS course feedback and an inner loop based on bank angle ϕ feedback, measured using an infrared inclinometer, are used to produce corrective actions by means of ailerons deflection δ_{ail} .

Also, in order to avoid flight conditions in which the capacity to control the vehicle is critically reduced, the wing bank reference angle is limited to $\pm 25^\circ$ by means of the saturation block depicted in Fig.6. This saturation mechanism is implemented in conjunction with the corresponding anti-windup strategy used in the calculation of the integral action in the PI controller.

An interesting aspect of the latero-directional control law is the use of integral action in the bank angle PID inner loop. Theoretically, if the ailerons deflection is such that $\delta_{ail} \neq 0$, this should produce angular rotation $d\phi/dt \neq 0$; i.e. there exists a natural integration from δ_{ail} to ϕ . However, in practice the ailerons can be incorrectly trimmed, or they can be asymmetrically mounted, such that it is necessary to produce non-zero ailerons deflection command even when $(\phi_{ref} - \phi) = 0$.

It is important to notice that course angle; which is related to the flight path executed by the aircraft center of mass; is not equal to yaw angle; which is the angle the aircraft body fixed reference frame forms with the north direction. These angles are equal only if the aircraft lateral velocity component is zero; i.e. only if the aircraft is not side slipping. Nevertheless, even if a particular SUAV mission demands the tracking of a reference yaw angle instead of course angle; e.g. in aircraft attitude based missions; GPS course angle measurements can sometimes be used, eliminating the need for a specific yaw angle sensor, such as a magnetometer. In the present

case, the pursued ground reconnaissance mission was proposed such that course angle is indeed the variable to be controlled.

As a final remark to the latero-directional control law, rudder control coordinated with ailerons deflection could have been used to improve the SUAV performance in curves. However, it was verified in simulation, and also in flight tests, that the SUAV aerodynamic characteristics (particularly the wings high dihedral angle) are such that rudder/aileron coordination does not lead to significant improvements in performance. Therefore, to reach a minimal complexity control structure, rudder deflection is not used in the current approach.

C. Control Hardware Description

From the above description of longitudinal and latero-directional control laws, it is possible to infer what sensors have been used in the hand-launched SUAV: (i) a high resolution digital baro-altimeter to measure altitude h ; (ii) a differential pressure sensor to measure dynamic pressure P_{dyn} ; (iii) an infrared (IR) inclinometer used to measure pitch θ and roll ϕ angles by means of indirect measurement differences in light intensity between ground and sky across the horizon line (9; 22); and (iv) a GPS receiver to measure geodesic position and course angle ψ . The main characteristics of these sensors are summarized in Table II.

Table II
HAND-LAUNCHED SUAV SENSORS CHARACTERISTICS.

Variable	Sensor	Characteristics
h	Baro- altimeter	SCP1000 – VTI Technologies. High resolution (up to 17 bits) digital absolute pressure sensor. Communication protocol: SPI. Range: 30kPa to 120kPa, and resolution of 6Pa (15 bits) for an update rate of 9Hz.
P_{dyn}	Differential pressure sensor	163PC01D75 – Honeywell. Analog sensor. Output: 1V to 6V. Range: $\pm 622\text{Pa}$ ($\pm 2.5'' \text{H}_2\text{O}$).
θ and ϕ	Infrared inclinometer	CPD4SEUNIT – FMA Direct. Analog sensor. Output: 1V to 5V after appropriate amplification by an instrumentation amplifier. Range: approx. $\pm 30^\circ$ in roll and pitch, depending on meteorological conditions.
ψ , latitude and longitude	GPS receiver	OEM GPS 18 – Garmin. Digital sensor. Communication protocol: NMEA over RS-232C. Update rate: 5Hz.

It is interesting to notice that the use of an infrared based attitude sensor leads to weight reduction together with smaller computational and financial costs when compared to traditional Inertial Measurement Unit (IMU) based solutions; even if MEMS accelerometers and gyros are used in the IMU. A more detailed exposition of the physics involved in the use of such infrared sensors is provided by (9). The main disadvantage of infrared based attitude estimation is the necessity of pre-flight recalibration due to the variation of the horizon thermal characteristics with meteorological conditions. Currently, an alternative procedure is under development to automatically recalibrate the infrared sensor from measurements of the local gravity acceleration vector prior to flight test.

Along with the set of sensors described above, other hardware components have been used to accomplish the mission requirements (Fig.7). All the communication is managed by two microcontrollers that receive and transmit data to and from a PDA bonded to the airplane cargo bay. The microcontrollers board also controls the redirection of pulse-width modulation (PWM) signals used to command the SUAV servos from PDA generated commands to radio-control received signals. This redirecting operation is started by a digital signal received from a specific channel by the onboard radio-control receiver, which is detected by one of the microcontrollers, through a digital input line (DIO in Fig.7), such that it can initiate the transfer from automatic to manual control, and vice-versa.

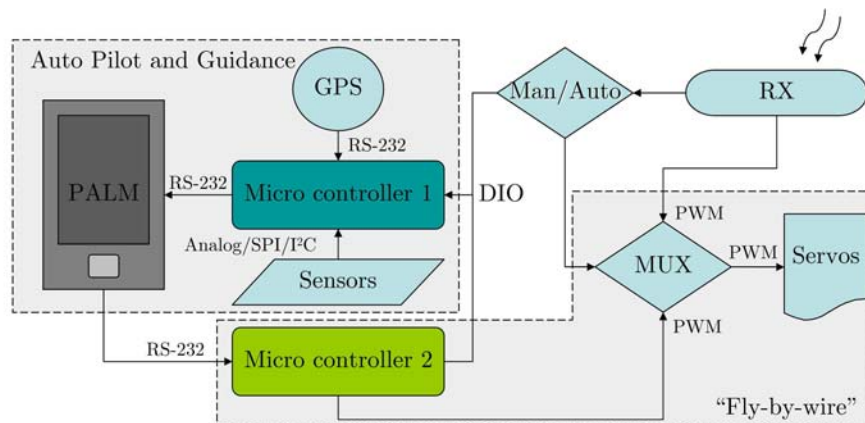


Figure 7. A detailed view of the control hardware. Note that the main device is a PDA that communicates with other devices through RS-232C shared serial bus.

The PDA used as the GN&C digital processing device in the hand-launched SUAV is a TX model manufactured by Palm Inc., with a 312MHz ARM-based processor, and 128Mb RAM, whose weight is 148.83g. The digital control laws are executed as a single thread, at a rate of 5Hz. The communication is performed by sharing the same RS-232C serial port to simultaneously transmit and receive data to and from different microcontrollers, as shown in Fig.7.

An analog 2.4GHz/200mW video downlink is established by using a commercial off-the-shelf video system for aircraft models, manufactured by Black Widow A/V LLC. The onboard camera and video transmitter are turned-on on ground, right before each flight. This video system weights only 42g.

V. SIMULATION ENVIRONMENT

An essential task in the development of GN&C strategies for UAVs is the construction of faithful simulators (8). A reliable simulation environment can help to dramatically reduce the number of costly trial-and-error experimental flights.

The SUAV simulation environment was implemented using the MATLAB/Simulink graphical language, developed by MathWorks Inc., and it was based on the assumption that the vehicle can be correctly represented as a rigid body with six degrees of freedom. In this case, the Newton laws of motion, considering a plane tangent to the earth surface as an approximate inertial frame, together with known kinematic relations, led to the flat-earth equations of motion (21) used to model the aircraft dynamical behavior.

As shown in Fig.8, the SUAV was represented as a mathematical model divided in four main subsystems: standard atmosphere, aerodynamics, propulsion and equations of motion.

In the *Standard Atmosphere subsystem* it is included the 1976 U.S. Standard Atmosphere Model (21), together with turbulence and nonzero mean wind field perturbations.

The forces and moments applied to the SUAV, as a result of the interaction of the vehicle with the air flow, are calculated in the *Aerodynamics subsystem*. The intensities of these aerodynamic forces and moments are determined mainly by the dynamic pressure (4) associated to the SUAV speed with respect to the atmosphere, such that the following general expressions can be written:

$$\begin{aligned} F_{\text{aero}} &= C_F P_{\text{dyn}}, \\ M_{\text{aero}} &= C_M l P_{\text{dyn}}; \end{aligned} \tag{5}$$

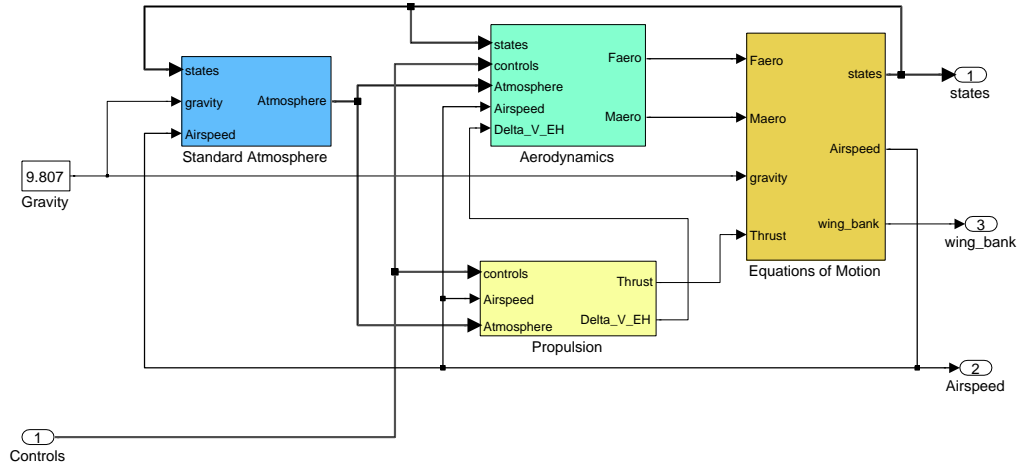


Figure 8. Simulation environment. The UAV was represented as a six degrees of freedom rigid body affected by forces resulting from interactions with atmosphere, propulsion and local constant gravity.

where C_F is a dimensionless aerodynamic coefficient associated to the lift, drag or lateral force; C_M is also a dimensionless coefficient associated to the roll, pitch or yaw moment; and l is a constant characteristic length. Actually, the C_F and C_M aerodynamic coefficients are functions of the aircraft geometry, vehicle attitude with respect to the airflow, and UAV control surfaces deflection. The accurate estimation of these functions is one of the main obstacles in the preparation of an aerial vehicle simulation environment.

In the present work, all the aerodynamic characteristics of the modified aircraft model, described in Section II, were calculated using a specific software – the CEA-VLM software – developed in the Center for Aeronautical Studies at the Universidade Federal de Minas Gerais – CEA/UFMG (23). Using this software, all aerodynamic coefficients, including nonlinear effects such as stall, were obtained by means of a modified vortex-lattice finite element method. The software includes calculation of induced drag on Trefftz-Plane and calculation of free-wake for all lift surfaces, together with the iterative use of airfoils experimental characteristics. This last feature allows the estimation of aerodynamic parameters beyond stalled conditions. The main advantage of this software is the use of a user-friendly interface in which the user can insert the geometry and airfoil distribution of the airplane, and the coefficients and derivatives for several operational conditions can be automatically calculated. The compiled version of this software

can be freely downloaded from the CEA/UFMG Internet web site².

In the *Propulsion subsystem*, aerodynamic thrust coefficients were calculated for the airplane propeller to faithfully represent the thrust force variation with airspeed and throttle command. Moreover, the effect of propeller downwash was appropriately accounted for in the simulation by establishing a connection between this subsystem and the *Aerodynamics subsystem* (Fig.8). However, the contribution of the electrical engine dynamical response was not included in the *propulsion subsystem* because it was considered unimportant to the overall aircraft dynamical behavior.

Once the forces and moments acting on the SUAV are calculated, and the vehicle mass and inertia matrix are known, a set of twelve nonlinear differential equations (21) can be integrated to produce the SUAV dynamical behavior. These equations were grouped in the *Equations of Motion subsystem* shown in Fig.8.

A sample of simulation results are shown in Fig.9 and Fig.10.

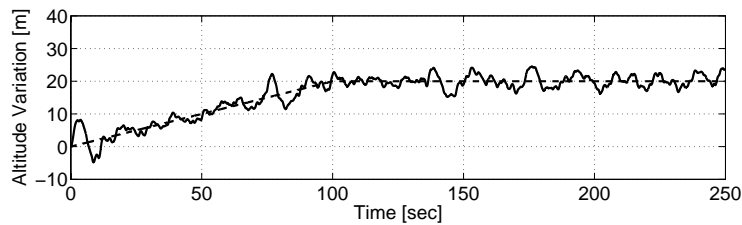


Figure 9. Typical simulation results obtained for longitudinal maneuver corresponding to a climb followed by levelled flight, including turbulence effects. This figure should be compared to Fig.11b.

VI. FLIGHT TESTS

Nowadays, the developed SUAV has more than one hundred flights using the guidance strategies described in Sections III-A and III-B. These flight tests were performed in diverse atmospheric circumstances from no wind and clear sky to high wind (about 30km/h) and clouded conditions.

²<http://www.demec.ufmg.br/Cea/>

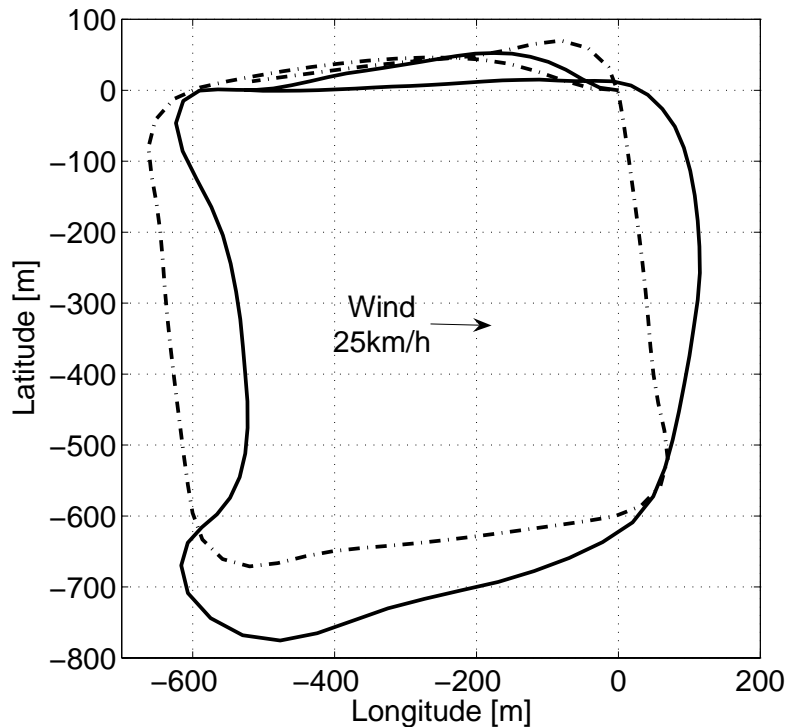


Figure 10. Typical simulation results using the switched vector field guidance methodology. Two situations are depicted for the same set of waypoints: the dash-dotted SUAV path corresponds to no wind condition; and the continuous path to a 25 km/h west to east constant wind.

In this section, typical results achieved in these flight tests are shown. These include results related to the altitude, course and airspeed control, together with examples of how the SUAV can be used to execute ground reconnaissance missions in pre-defined areas.

Figure 11 presents a typical altitude trajectory tracking result obtained relying on the closed loop control structure depicted in Fig. 5. The implemented controller was able to execute a 20 m climb in 100 s, followed by levelled flight. During this mission, the maximum altitude error was 7 m, which was observed to be smaller than the error obtained during SUAV manual control, when piloted by an experienced human pilot. The high variation rate observed in the elevator deflection is a result of the pitch rate stabilization augmentation control together with atmospheric gusts in the real environment. A comparison between Fig. 11 and Fig. 9 reveals that the simulation environment described in Section V seems to be faithful.

The aircraft speed control performance in keeping a constant dynamic pressure during the

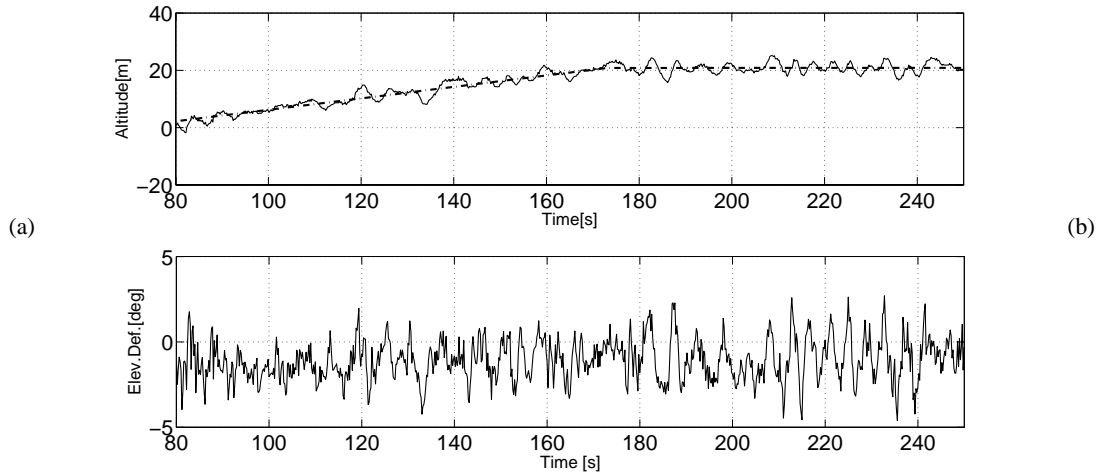


Figure 11. SUAV longitudinal control real result corresponding to 20 m climb followed by levelled flight. (a) Altitude variation (the dash-dotted line represents the reference and the continuous one the measured signal). (b) Elevator deflection (control action).

entire flight test can be evaluated by examining the typical result presented in Fig. 12. Although variations of ± 50 Pa are considered negligible in the present case, significant variations were also observed ($t \approx 180$ s; $t \approx 195$ s and $t \approx 205$ s). These variations were mainly due to wind disturbances in the real environment, together with the fact that there is no airbrake system to slow down the aircraft during events of abrupt buildup of dynamic pressure.

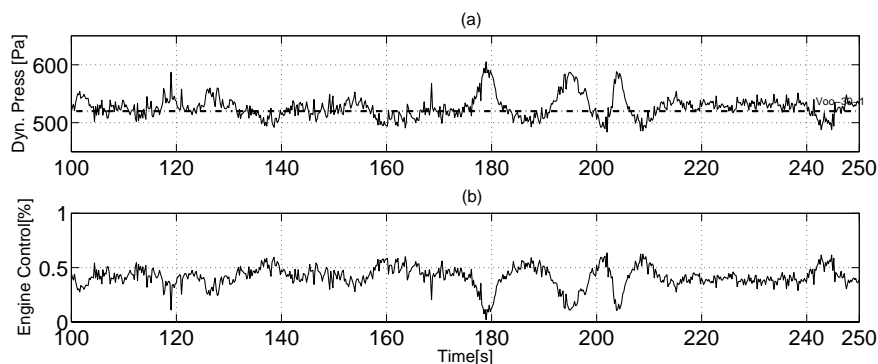


Figure 12. SUAV longitudinal control real result corresponding to the regulation of the vehicle airspeed. (a) Dynamic pressure variation (the dash-dotted line represents the reference and the continuous one the measured signal). (b) Normalized engine command (control action).

Using the latero-directional control strategies described in Section IV-B it was also possible to achieve good results, a sample of which are shown in Figs. 13 and 14. As discussed previously, the roll angle ϕ is controlled to effect desired changes in the course angle ψ , in order to follow a reference signal ψ_{ref} determined by one of the guidance procedures presented in Section III.

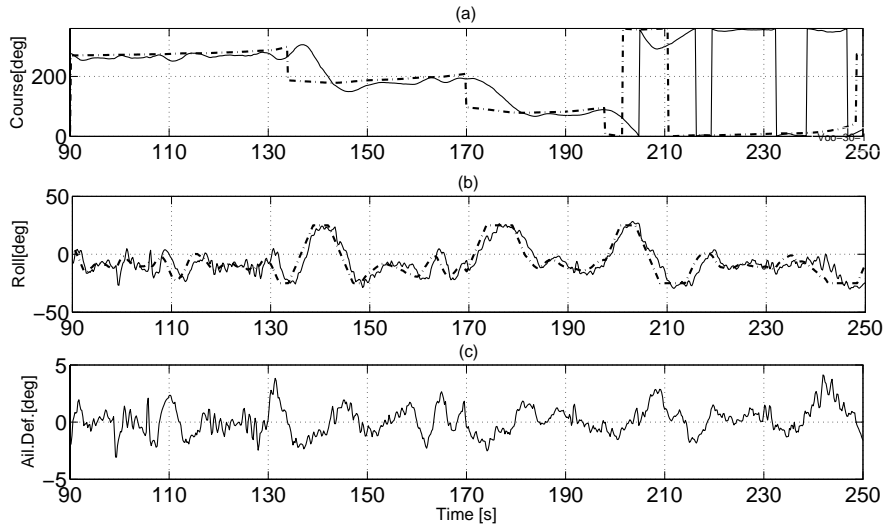


Figure 13. SUAV latero-directional control real result using the switched vector field guidance strategy. (a) Course angle variation and (b) roll angle effected to follow the prescribed trajectory: the dash-dotted lines represent reference signals and the continuous ones are the measured signals. (c) Ailerons deflection.

A comparison of the results obtained using the switched (Fig. 13) and continuous (Fig. 14) vector field guidance strategies reveals that the former alternative induces undesirable transient behaviors not present when the continuous vector field guidance procedure is employed. This can be clearly observed during the time intervals $132\text{ s} \leq t \leq 170\text{ s}$, $170\text{ s} \leq t \leq 195\text{ s}$ shown in Fig.13a. It is important to notice that some discontinuities shown in Fig. 13a, and all discontinuities observed in Fig. 14a, are indeed artificially introduced by the crossing of signals beyond the 360° limit.

Figure 15 presents a typical trajectory achieved by the SUAV during a flight test. The mission consisted of two laps in a square and flat area determined by four relative waypoints, distant 600 m apart from each other, and previously chosen and recorded in the PDA onboard software. The initial point is automatically assumed to be the position corresponding to the time instant when the autonomous guidance strategy is engaged by the issuing of a remote command from

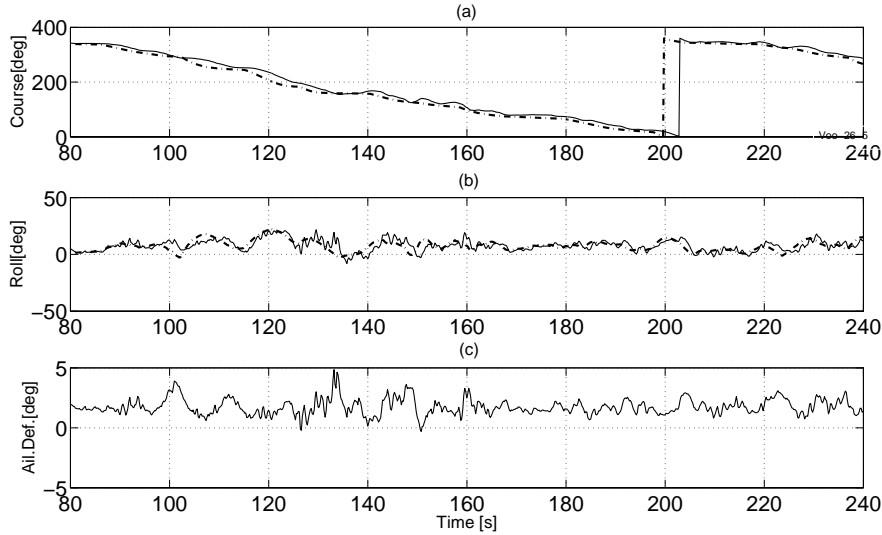


Figure 14. UAV latero-directional control real result using the continuous vector field guidance strategy. (a) Course angle variation and (b) roll angle effected to follow the prescribed trajectory: the dash-dotted lines represent reference signals and the continuous traces are measured signals. The apparent discontinuities are not real but instead produced by the crossing of the 360° limit. (c) Ailerons deflection.

the operator.

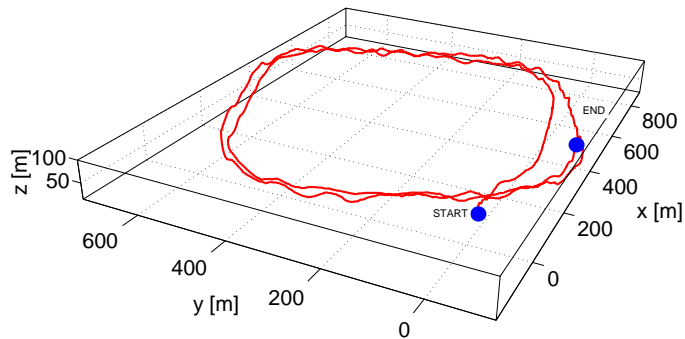


Figure 15. Typical flight mission executed by the UAV using the continuous vector field guidance strategy. The UAV trajectory start and end points are indicated in the figure.

It is interesting to notice, in Fig. 15, the repeatability of the UAV. The executed trajectory in the second lap almost coincides with the flight path accomplished in the first lap.

In Fig. 16, another comparison related to the use of switched or continuous vector field

guidance procedures is presented. The trajectory executed following the continuous vector field approach remains entirely inside the corridor delimited by the two concentric squares shown in the figure. For both strategies it is observed overshoot on the corners of the tunnel, particularly on the corner associated to the waypoint 4, where a tail-wind condition almost prevents the correct execution of the turning maneuver. On the other hand, it is conjectured that these deviations on the corners could become negligible for greater distances between waypoints. Despite this fact, in the continuous vector field strategy the resulting trajectory is smoother than in the switched vector field approach, as it can be verified through the comparison between minimum turning radius observed in each case.

The above results seem to indicate that, although both strategies would perform similarly in some general missions, the use of continuous vector field guidance approach is recommended in problems where the SUAV should remain constrained to a virtual corridor or tunnel in the sky; e.g. in the monitoring and surveillance of roads, rivers and oil pipelines.

Figure 17 presents the ultimate result of a typical ground reconnaissance mission performed by the SUAV system. As described in Section IV-C, a commercial off-the-shelf video system is used to transmit images to the ground, where they are recorded to be processed later on. Therefore, the image mosaicing was manually performed off-line; although the authors are currently improving a method to automatically execute this task on-line. The result shown in Fig. 17 implies that missions related to the observation of large structures on ground; such as airports, roads, ships, etc; can be seamlessly accomplished by the hand-launched SUAV described in the present paper.

VII. FINAL REMARKS

This paper presented the main aspects of the development of a hand-launched small UAV to be used in ground reconnaissance missions. A commercial sailplane model, modified to act as a motor glider, was used as the aerial platform. Besides hardware integration, details of the guidance strategies and controllers used in the SUAV were presented in the paper. Real data obtained from several flight tests were used to illustrate performance details of the SUAV guidance and control system.

Although the paper discussed around the development of a specific SUAV, the authors believe that some aspects of the presented methodology are contributions to the field of unmanned air vehicles. These contributions are: (i) the continuous vector field guidance methodology presented

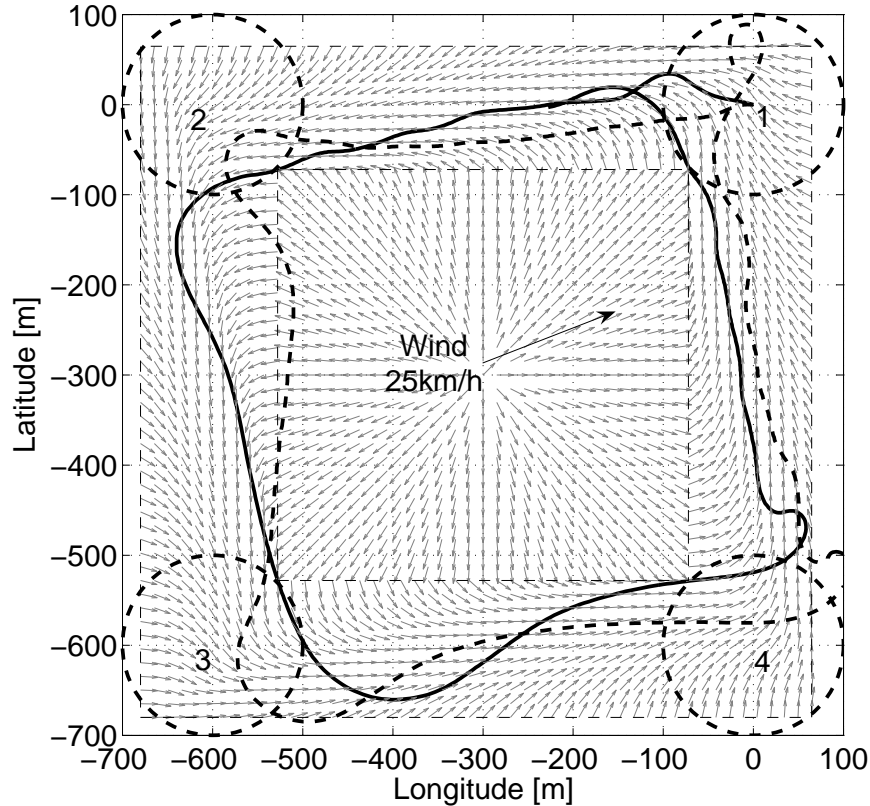


Figure 16. Comparison between typical trajectories obtained with switched (dashed thick line) and continuous (continuous thick line) vector field guidance strategies, on a typical day with 25 km/h wind in the direction shown in the figure. On the figure background the computed vector field is also displayed as a set of small arrows, together with a virtual tunnel or corridor formed by two concentric squares drawn using dashed thin lines. The great circles on the tunnel corners, numbered 1 to 4, correspond to areas around predefined waypoints.

in the paper, together with its evaluation in a real environment; and (ii) the non-traditional control hardware setup, and simple control structure design, that proved to be sufficient for the accomplishment of the SUAV ground reconnaissance mission.

The guidance strategy based on continuous vector field proved to be very adequate to reconnaissance missions, especially because it generates a smooth course reference inside a polygonal corridor. This corridor could, for example, be defined such that it includes a road or a river to be surveyed. A limitation of this approach is that it does not explicitly considers the airplane altitude, which must be considered independently by the controller.



Figure 17. Image mosaicing as the ultimate result of a typical mission accomplished by the hand-launched SUAV.

There are several important directions for future work. On the vehicle controller design methodology it is important to rigorously determine the minimal amount of sensors necessary to control the UAV in order to be able to augment the payload. Also, fault detection and emergency procedures must be added to improve the system safety. As for guidance and mission control, the authors are currently developing vector field methodologies that account for three dimensional configuration spaces. Automatic waypoint determination algorithms that consider fixed obstacles, such as mountains and forbidden areas, must also be addressed. Regarding the mission itself, it is essential to construct image-processing tools that are able to perform automatic image correction and mosaicing. A software with this characteristics is currently under development and it will be published in the future.

ACKNOWLEDGMENTS

The authors would like to thank the financial support from Fundação de Amparo à Pesquisa do Estado de Minas Gerais – FAPEMIG and Conselho Nacional de Desenvolvimento Científico e Tecnológico – CNPq, Brazil.

REFERENCES

- [1] Micropilot, “MP2028 autopilot series,” <http://www.micropilot.com>, 2007, last access in January, 2008.
- [2] CloudCap, “Piccolo autopilot system,” <http://www.cloudcaptech.com>, 2007, last access in January, 2008.

- [3] Crossbow, “MNAV100CA with stargate processor,” <http://www.xbow.com>, 2007, last access in January, 2008.
- [4] J. Ryu and J. C. Gerdes, “Integrating inertial sensors with GPS for vehicle dynamics and control,” *Journal of Dynamics Systems, Measurement and Control*, vol. 126, no. 2, pp. 243–254, 2004.
- [5] N. S. Kumar and T. Jann, “Estimation of attitudes from a low-cost miniaturized inertial platform using kalman filter-based sensor fusion algorithm,” *Sadhana-academy Proceedings in Engineering Sciences*, vol. 29, no. 2, pp. 217–235, 2004.
- [6] S. Laparra and J. Angel, “Low cost navigation system for UAVs,” *Aerospace Science and Technology*, vol. 9, pp. 504–516, 2005.
- [7] D. Gebre-Egziabher, “Design of multi-sensor attitude determination systems,” *IEEE Trans. on Aerospace and Electronic Systems*, vol. 40, no. 2, pp. 627–649, 2004.
- [8] E. Johnson and S. Fontaine, “Use of flight simulation to complement flight testing of low-cost UAVs,” in *AIAA Modeling and Simulation Technologies Conference*, 2001.
- [9] B. Taylor, C. Bil, S. Watkins, and G. Egan, “Horizon sensing attitude stabilization: A VMC autopilot,” in *18th International UAV Systems Conference*, Bristol, UK, 2003.
- [10] J. J. Kehoe, “Autopilot development for a micro air vehicle using vision-based attitude estimation,” Master’s thesis, University of Florida, 2004.
- [11] P. Iscold, “Development of a small unmanned air vehicle,” *SAE Technical Papers*, no. 2007-01-2734, 2007.
- [12] R. Rysdyk, “UAV path following for constant line-of-sight,” in *Proceedings of the 2nd AIAA Unmanned Unlimited Systems, Technologies, and Operations - Aerospace*, 2003.
- [13] M. Breivik and T. I. Fossen, “Principles of guidance-based path following in 2d and 3d,” in *Proc. of the IEEE Conference on Decision and Control*, 2005, pp. 627–634.
- [14] O. Khatib, “Real-time obstacle avoidance for manipulators and mobile robots,” *Int. J. Robot. Res.*, vol. 5, no. 1, pp. 90–98, 1986.
- [15] D. Lawrence, “Lyapunov fields for UAV flock coordination,” in *Proceedings of the 2nd AIAA Unmanned Unlimited Systems, Technologies, and Operations - Aerospace*, 2003.
- [16] E. W. Frew, D. A. Lawrence, C. Dixon, J. Elston, and W. J. Pisano, “Lyapunov guidance vector fields for unmanned aircraft applications,” in *Proc. of the American Control Conference*, 2007, pp. 371–376.

- [17] J. Osborne and R. Rysdyk, "Waypoint guidance for small UAVs in wind," in *Proceedings of the AIAA Infotech, Aerospace Conference*, 2005.
- [18] C. Belta, V. Isler, and G. J. Pappas, "Discrete abstractions for robot motion planning and control in polygonal environments," *IEEE Transactions on Robotics*, vol. 21, no. 5, pp. 864–874, October 2005.
- [19] G. A. S. Pereira, L. C. A. Pimenta, L. Chaimowicz, A. R. Fonseca, D. S. C. de Almeida, L. de Q. Corrêa, R. C. Mesquita, and M. F. M. Campos, "Robot navigation in multi-terrain outdoor environments," in *Experimental Robotics: The 10th International Symposium on Experimental Robotics*, O. Khatib, V. Kumar, and D. Rus, Eds. Springer, 2008, pp. 331–342.
- [20] L. C. A. Pimenta, G. A. S. Pereira, and R. C. Mesquita, "Fully continuous vector fields for mobile robot navigation on sequences of discrete triangular regions," in *Proc. IEEE Int. Conf. Robot. Automat.*, 2007, pp. 1992–1997.
- [21] B. L. Stevens and F. L. Lewis, *Aircraft Control and Simulation*. John Wiley & sons, Inc., 2003.
- [22] A. Kawalec, W. Komorniczak, J. Pietrasinski, and W. Czarnecki, "Evaluation of a low-cost microUAV platform for sensor suite," in *Proc. of the IEEE International Radar Symposium – IRS*, Krakow, Poland, 2006, pp. 1–4.
- [23] P. Iscold and L. A. T. de Vargas, "A fast aerodynamic procedure for a complete aircraft design," *SAE Technical Papers*, no. 2006-01-2818, 2006.